NUMERICAL SIMULATION OF THE BEARING FAILURE MECHANISM OF THIN-PLY METAL LAMINATES

B. Kötter[1], K. Yamada[2], N. Takatsuka[1], B. Fiedler[3] and M. Nishikawa[1]

[1] Department of Mechanical Engineering and Science, Kyoto University, Kyoto, Japan,
koetter.benedikt.25z@st.kyoto-u.ac.jp, www.me.t.kyoto-u.ac.jp
[2] Industrial Technology Center of Fukui Prefecture, Fukui, Japan, www.fklab.fukui.fukui.jp/kougi/
[3] Institute of Polymers and Composites, Hamburg University of Technology, Hamburg, Germany,
www.tuhh.de/kvweb/home

Keywords: Thin-Ply, Fibre Metal Laminates, FEM, Bolt Connection, Hybrid Composites

ABSTRACT

Within this study, the influence of a local hybridisation of Thin- and Thick-Ply laminates under bearing conditions was investigated by numerical simulations. The hybridisation was carried out by substituting 90° layers with stainless steel patches locally in the area of the load introduction. The stainless steel patches or foils had the same thickness as the prepreg layers. This prevents any unintentional change or disturbance of the laminate geometries. The CompDam - Deformation Gradient Decomposition (DGD) damage model was chosen for the numerical investigations. The study results showed that a reduction in layer thickness is associated with increased bearing strength. The bearing strength improvement of hybrid specimens is significantly higher for Thin- and Thick-Ply specimens. An improvement of almost 50 % could be achieved. Fibre kinking led to final failure for all configurations. The initiation of fibre kinking occurred in the 0° layers, which has the highest compressive stress. However, it could be observed that using stainless steel patches reduces the maximum compressive stress in the middle 0° layer. Thus, the initiation of fibre kinking shifted to higher strains or stresses, resulting in a higher bearing strength.

1 INTRODUCTION

Due to their density-specific mechanical properties, design flexibility and superior properties under cyclic loading compared to conventional metals, fibre composites are increasingly used as structural materials [1].

However, with conventional composites, as they are used today, the full potential of the carbon fibres cannot be exploited. Composites usually fail due to pre-damage, such as delamination. To increase the performance of carbon fibre composites, one possibility is to reduce the layer thickness of a single prepreg layer. Thin-Ply prepregs are characterised by a layer thickness of less than 100 µm [2]. Previously, layer thicknesses of up to 18 µm have been experimentally investigated. The reduction of the layer thickness increases the freedom of design. Due to the increased number of layers, the laminate layup can be designed to be more load-dependent. In addition to the degree of freedom in design, the fibre spreading process improves the quality of the prepreg layers. Thin-ply prepregs are characterised by a more homogeneous fibre distribution and smaller and less resin-rich regions [3]. Several studies have focused on the mechanical properties of quasi-isotropic laminates as a function of layer thickness. They show increasing tensile and compressive strengths with decreasing layer thickness [2–5]. In a study by Amacher et al., an increase of 42 % in tensile strength was measured for quasi-isotropic specimens [3]. The fracture strain of the samples was nearly the same as the fracture strain of the carbon fibres used. Almost the full potential of the carbon fibres was utilised. In addition to the increase in strength, a shift of the damage initiation to higher strains or stresses was also observed, and the initiation and growth of delamination were suppressed. The failure behaviour changes from a delamination dominated for Thick-Ply laminates to a brittle, fibre-dominated failure behaviour for Thin-Ply laminates.

To exploit the full lightweight potential of Thin-Ply laminates for future applications, it is essential to investigate the bearing behaviour. Bolt connections are one of the main techniques for joining two or more parts. But due to the lower bearing and shear strength, the higher notch sensitivity, the non-

isotropic material properties, and the dependence of the failure mechanisms on the laminate structure, the effort required to design a composite bolt connection is significantly higher than for metals [2,6]. Studies showed an increase in bearing strength with decreasing layer thickness of about 18 %, but the improvement is significantly less than in tensile and compressive strengths [3,7,8]. Therefore, bolt connections are a limiting factor for future Thin-Ply composite applications.

Various methods are available to increase the bolt performance of a composite material. These include the local thickening of the laminate, placing inserts or Z-pinning [6,9–11]. The present study investigates the ply substitution technique to improve the bearing performance. Metal foils substitute the 90° layers locally in the area of stress concentrations (see Figure 1).
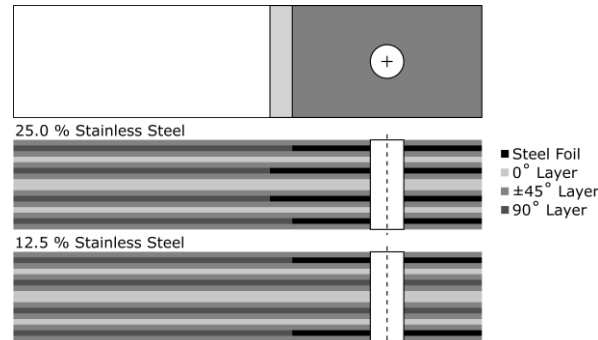

Figure 1: Schematic drawing of the ply substitution method; 90° CFRP layers are locally substituted in the area of stress concentrations by stainless steel patches

Experimental studies showed that due to the hybridisation, the bearing strength increased significantly, and the sensitivity of the mechanical properties to the laminate configuration and environmental effects decreased [6,8]. Fink et al. investigated the hybridisation of CFRP laminates due to titanium foils [9]. Their study exhibits an increase in the bearing strength of a three-row bolt connection by 91 % with a local titanium content of 20 %.

In 2009, Camanho et al. published a study on the numerical simulation of bearing properties of hybrid composites using titanium as reinforcement material [6]. They used a progressive damage model implemented in Abaqus. Damage initiation was determined using the Hashin criterion [12], and the damage propagation was based on the material strength for each failure mode to guarantee a mesh-independent result. The results show that the numerical models developed can predict the maximum ultimate load. According to Camanho et al., larger deviations can be explained by the fact that they assume a plane stress state and stresses perpendicular to the laminate are not included in the simulation. Furthermore, the model does not consider the influence of shear stresses on the onset of fibre buckling. However, shear stresses are essential in fibre buckling [13]. In 2022, three studies were published in numerical simulation of composites' bearing properties, which all used a three-dimensional stress state. However, each of them used a different numerical approach. Wang et al. investigated the failure mechanisms with a three-dimensional progressive failure mode and implemented a subroutine UMAT in Abaqus Standard [14]. The failure model considers the matrix crack orientation, matrix crack closure effect, interface delamination and damage propagation. The intralaminar damage onset was determined by the Hashin and Mohr-Coulomb criteria [12,15]. The numerical results showed a good agreement regarding stiffness and maximum strength.

In contrast, Wang et al. used Abaqus Explicit and implemented a VUMAT based on the three-dimensional LaRC failure model [16]. The LaRC model distinguishes different initial failure modes: Fibre tension, fibre kinking, non-linear shear, matrix tensile and compressive failure. The model very well reproduced the damage mechanisms, the initiation, and the strength of the experimental tests. Zhuang et al. also used Abaqus Explicit and implemented a VUMAT [17] to simulate cross-ply and angle-ply composites. For the prediction of the damage initiation, the transversely isotropic invariant-based criteria was used for compressive failure and the maximum strain criteria for the tensile failure.

A bi-linear damage model and smeared crack model were implemented to simulate the post-peak intralaminar damage evolution. The simulation achieved good agreement with the experimental results. The results exhibited that shear non-linearity is one of the most critical factors for predicting bearing behaviour.

This study aims not to develop a new failure model regarding the failure mechanism under bearing but to investigate the effects of local hybridisation of composites with metal foils. Previous experimental studies have shown that fibre kinking leads to the final failure [8]. For this reason, the continuous damage model "CompDam-DGD" was chosen for the numerical investigations since the buckling theory from Budiansky is implemented in the model [18].

2 CONTINUUM DAMAGE MODEL

The CompDam - Deformation Gradient Decomposition (DGD) damage model represents the damage at the mesoscale level of fibre composites, describing each composite layer individually [18]. The CDM material model is implemented as an Abaqus/Explicit User Subroutine (VUMAT) to simulate cracks in the matrix under tensile, compressive and shear loading, fibre fractures under tensile and compressive loading and fibre kinking. The kinematics of matrix cracks is calculated according to the deformation gradient decomposition approach [19]. The fibre tensile damage is modelled with the conventional CDM strain softening method. The fibre kinking model is based on Budiansky's fibre buckling theory, which describes the kink band initiation and propagation [20,21].

The following briefly introduces the fibre kinking theory from Budiansky, as fibre kinking was the decisive factor for selecting the continuum damage model CompDam-DGD. For further details on damage initiation or propagation of other failure criteria, please refer to the following publications [19,22–26].

The fibre kinking theory (FKT) describes the mechanical response behaviour of a composite layer when fibre kinking occurs. Important parameters are the fibre misalignment, the non-linear shear stress-strain behaviour, and the fibre rotation due to deformation [27]. The typical response behaviour within the initiation of a kink band is shown in Figure 2. The kink band initiation occurs as soon as the compressive strength X_C is reached. The stress drops suddenly until it reaches a certain level. This stress level is called crush stress [28]. On the right side of Figure 2, an idealised kink band is schematically shown with the kink band angle β, the fibre misalignment angle φ and the kink band width w_{kb}.
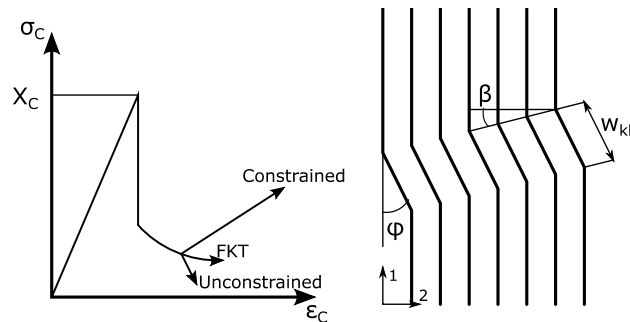

Figure 2: Mechanical fibre kinking response and schematic view of a kink band

Assuming that the shear non-linearity of a layer is described according to Ramberg-Osgood [28], the stress of initiation of the kink band results from Eq. 1. G_{12} is the in-plane shear modulus, α and η define the shear stress-strain behaviour, and φ_0 describes the initial fibre misalignment.

$$X_C = \frac{G_{12}}{1 + \eta \cdot \alpha^{1/\eta} \cdot \left(\frac{G_{12} \cdot \varphi_0}{\eta - 1}\right)^{\frac{\eta-1}{\eta}}} \tag{1}$$

After initiation of the kink band, large deformations of the fibres occur. These deformations lead to large bending stresses, resulting in the fracture of the fibres. Different post-peak behaviours can occur if the fibres break, depending on the surrounding conditions, as shown in Figure 2 on the left. If the layer is unconstrained, the composite undergoes frictional sliding. The longitudinal stress increases if the material is constrained due to, for example, other layers. The fibre fracture angle indicates the fibre rotation at which the fibres break due to high bending stresses. In this study, a fibre fracture angle of $\varphi_{ff} = 10°$ is chosen, following the publication by Bergan et al. [22].

3   NUMERICAL SIMULATIONS

The numerical simulations are bearing tests according to ASTM D5961 [29]. The load is applied using a metal bolt with a diameter D of 6 mm. The surfaces of the specimen near the bolt are clamped due to washers on both sides, see Figure 3. The other end of the specimen is fixed. The bolt strength σ^{br} is calculated as shown in Equation 2.

$$\sigma^{br} = \frac{P}{k \cdot D \cdot h} \tag{2}$$

P is the load, h is the specimen thickness, and k is the load per hole factor; 1.0 for single-fastener or pin tests and 2.0 for double-fastener tests. The calculation of the bearing strain ε^{br} is shown in Equation 3.

$$\epsilon^{br} = \frac{(\delta_1 + \delta_2)/2}{K \cdot D} \tag{3}$$

δ_1 and δ_2 are the local displacements, as shown in the schematic test setup in Figure 3. K is the calculation factor to distinguish single-shear from double-shear tests. For double-shear tests, the calculation factor K is 1.0 and for single-shear tests 2.0. The test setup within this study is a double-shear test with one bolt. In addition to the schematic drawing of the test setup, the specimen geometries used are shown in Figure 3. Compared to the ASTM standard, the length of the specimen was reduced from 135 mm to 80 mm.
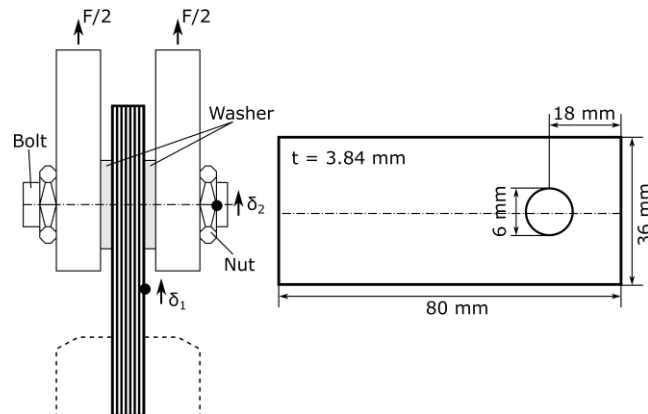

Figure 3: Schematic drawing of the test setup and specimen dimensions

3.1 Material properties

The composite material used for the simulation is a prepreg system consisting of TR50S carbon fibres from Mitsubishi Chemical Co., Ltd. and a bisphenol-A based epoxy resin from a combination of jER828:jER1001 in a 4:6 ratio from Mitsubishi Chemical Co., Ltd. The material properties and parameters were already investigated in previous works and adopted for this study [8,30,31].

The austenitic stainless-steel alloy 1.4310 (X10CrNi18-8) was used as substitute layers. The alloy 1.4310 is characterised by high strength and ductility and exhibits good corrosion properties. The

thicknesses of the foils are the same as the prepreg layers. The material properties of the CFRP layers, the stainless-steel foil and the fracture toughness are reported in Tables 1, 2 and 3.

E_1 (MPa)	E_2 (MPa)	G_{12} (MPa)	G_{23} (MPa)	ν_{12}	ν_{23}
117000	8350	3960	2879	0.38	0.45

X_T (MPa)	X_C (MPa)	Y_T (MPa)	Y_C (MPa)	S_L (MPa)	
2333	985	62	163	97.6	

Table 1: Ply elastic properties and strength; G_{23} was calculated as $E_{22}/(2(1+\nu_{23}))$

	Steel - CFRP	CFRP – CFRP
G_{Ic} (J/m^2)	202	180
G_{IIc} (J/m^2)	2353	575

Table 2: Interlaminar fracture toughness; The data were determined experimentally by double cantilever beam (Mode I) [32] and end-notched flexure tests (Mode II) [33]

E (GPa)	σ_Y (MPa)	ε_Y (%)
172.6	1273	1.176

Table 3: Mechanical properties of the stainless-steel foil; The data were determined experimentally by tensile tests according to ASTM E345-16 [34]

The stainless-steel patches substitute the 90° prepreg layer locally in the stress concentration region, even in practical use. If the steel content is lower than 25 %, the outer 90°layers are replaced by steel foils. To minimise a locally increased stiffness due to the insertion of stainless-steel patches, the steel patches have different lengths and are arranged stepwise, as shown in Figure 1. Two layer thicknesses of 40 µm and 160 µm were examined. In both cases, reference samples without stainless steel and samples with a local steel content of 25 vol.-% stainless steel foil were simulated.

3.2 Finite element model

To reduce the computation time, one FEM model with the same dimensions as the tested samples was used to validate the FEM Model. Further simulations concerning the hybridisation are carried out on FEM models with a thinner laminate thickness and smaller dimensions.

The simulation model setup for validation is shown in Figure *4*: FEM model to validate the damage model and the used material parameter; In the load application area, the mesh is finer to minimise convergence problems.. A Python script creates the model, which can be imported into Abaqus. The dimensions of the samples are 80x36x3.84 mm. In contrast to the experimental tests, the dimensions differ in the length of the samples to reduce the calculation time. According to the standard and the experimental work, a quasi-isotropic laminate structure is used. In the case of hybridisation, a certain proportion of the 90° layers are substituted by stainless steel foils across the entire specimen length. As a result, the transition zone between the stainless steel foil and the 90° CFRP layers was not required to simulate, reducing the calculation time. Each layer has meshed separately with eight-node brick elements with reduced integration (C3D8R). In the area of the bolt, the mesh is refined, see Figure 4. The average edge length of the elements near the bolt is 0.16 mm. One element per ply is used along the thickness direction, whereby the coupling of the layers (CFRP-CFRP and CFRP-steel) is described with cohesive contact. The stainless-steel foils and the bolt are described with C3D8R elements. The material

behaviour of the steel of the bolt elements is linearly elastic without damage and degradation. The steel layers were modelled as elastic-plastic material behaviour using a Johnson Cook formulation [35]. The Johnson-Cook parameters were determined experimentally. The general contact algorithm from Abaqus/Explicit describes the contact between the CFRP-CFRP and CFRP-steel layer interfaces. New contacts throughout the simulation are allowed, and friction is considered. The friction coefficient between CFRP and CFRP is 0.2, and 0.3 between CFRP and steel. Surface-to-surface contact pairs were assigned to the contact between the CFRP or steel foils and the bolt. A penalty contact algorithm for the constraint enforcement and finite sliding were used to minimise the contact penetration between the layer and the bolt elements.
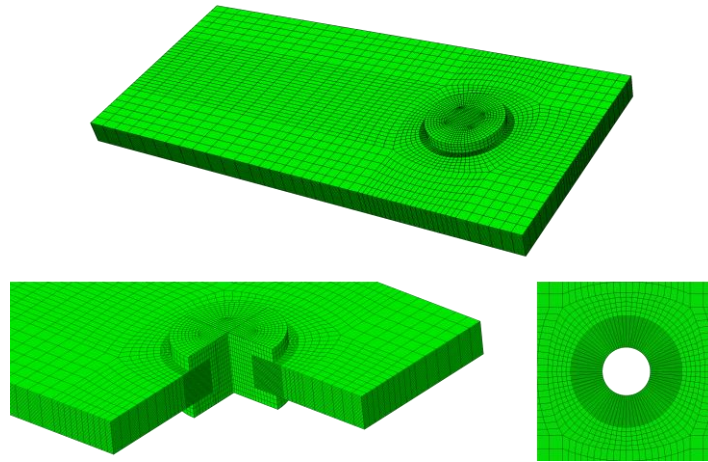

Figure 4: FEM model to validate the damage model and the used material parameter; In the load application area, the mesh is finer to minimise convergence problems.

4. RESULTS AND DISCUSSION OF THE NUMERICAL SIMULATIONS

As already described, the Thick-Ply reference sample was examined to validate the continuum damage model and the material parameters. The Thin-Ply and the hybrid samples were simulated using smaller samples with a thinner laminate thickness of 1.28 mm instead of 3.84 mm, reducing the calculation time. In the following Section 4.1, the results of the validation are described. In Section 4.2, the configurations are compared, and the failure behaviour of the hybrid specimens is examined in more detail.

4.1 Validation of the FEM bearing model

Figure 5 shows the stress-strain curves of the simulation as well as the experimental tests of a Thick-Ply reference sample. The experimentally determined stress-strain curve is shown in dark blue. In the area of low stresses, no linear behaviour is observed, whereby no damage is expected. The non-linear behaviour results from the clamping system used. Since this type of clamping system is not represented in the simulation, the dark blue curve should be modified. The linear section is extended to the Y-axis and the curve is shifted to the left by the amount of the intersection with the Y-axis. The shifted curve is shown in light blue. The stiffness of the tested sample is in agreement with the stiffness of the simulation, shown in black. The maximum bearing strength is also well reproduced by the model. However, the behaviour after failure cannot be represented. Due to large distortions of the elements, it is not possible to reproduce the post-failure behaviour with the current simulation model.
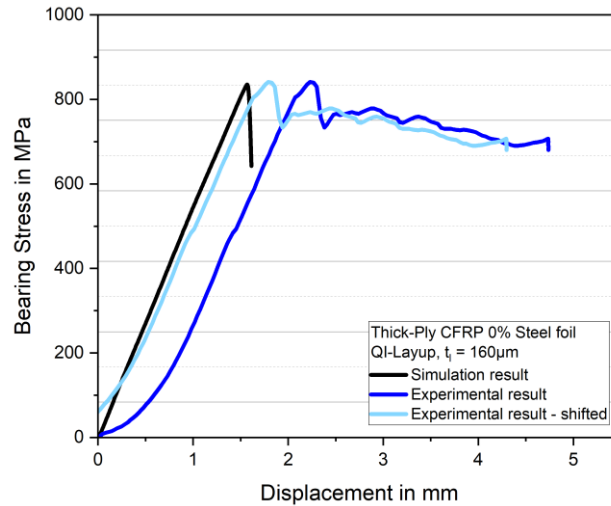
Figure 5: Comparison of bearing stress-displacement curves between the experiments (light and dark blue) and the simulation (black); The corresponding stress distributions in load direction and local fibre rotations are shown in Figure 6

The mechanical tests have shown that fibre buckling has led to final failure. The simulation results demonstrate these effects too. Figure 6 a) shows a sectional view of the FEM model. Figures 6 b) to e) present a part of this sectional view with the stress distribution in the load direction. The 0° layers show the highest compressive stresses (Figure 6 b) to d)). Due to the high compressive stresses, the layers buckle, as shown in Figure 6 d), which demonstrates the moment short after the maximum bearing stress (see black curve Figure 5). The initiation of the kink band occurs in the middle 0° layers and grows perpendicular to the laminate as the load increases. In Figure 6 d), the kink band extends from 3rd layer to 19th layer. In Figure 6 e), only the upper 0° layer still shows high compressive stress. Figure 6 e) correspond to the end of the black curve of Figure 5. According to Budiansky's buckling theory, all other 0° layers are already kinked and exhibit the crush stress as implemented. Due to the high contact forces between the bolt and the CFRP and the large deformations of the elements, a further calculation after the point in time shown in Figure 6 e) is currently not possible with the used FEM model.
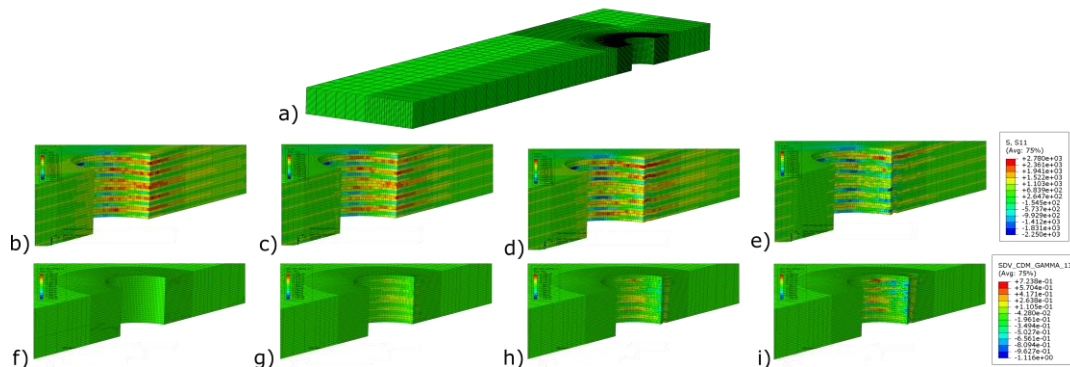

Figure 6: a) Section view of the FEM model; b-e) Stress distribution in load direction (σ_{11}) with increasing load; f-i) Fibre rotation angle int the 1-3 plane with increasing load, dark blue and red areas are representing broken fibres due to large deformation in the area of the kink band

Figures 6 f) to i) show the fibre rotation in the 1-3 plane. The dark blue and red areas represent a

fibre rotation angle of 10° respectively -10°. 10° fibre rotation represents the maximum value, corresponding to the fibre fracture angle φ_{ff} used. As a result, once the φ_{ff} fibre rotation is reached, the fibres will break, and the stress will drop to the crush stress, see Figure *2*. In Figure 6 h) and i), the kink band is clearly visible by the fracture of the fibres along a line perpendicular to the laminate.

4.2 Bearing behaviour of hybrid Thin- and Thick-Ply laminates

Table 4 compares the simulation results of the samples with thinner laminate thickness and the results of the experimental work. The strength differences of the specimens without stainless steel are significantly larger compared to the simulations of the thicker laminates. The differences are 22.3 % for the Thin-Ply specimens respectively 26.8 % for the Thick-Ply specimens. The larger differences can probably be attributed to the changing geometry. Especially in the case of buckling, a stability problem can occur. Due to the thinner laminates, the middle layers are more constrained, resulting in higher bearing strength. With increasing steel content, the differences between simulation and experiment decrease. This might be due to the material properties of the stainless steel. The steel foil supports the layers against buckling. Therefore, the thickness of the laminate has less influence on the bearing strength.

Configuration	Bearing strength σ_{br} in MPa		Error
	Simulation	Experiment	
Thick-Ply Reference	1078	849.9	+26.8 %
Thick-Ply; 25.0 vol.-% SF	1552	1470.6	+5.5 %
Thin-Ply Reference	1198	979.6	+22.3 %
Thin-Ply 6.25 vol.-% SF	1290	1165.4	+10.7 %
Thin-Ply 12.5 vol.-% SF	1357	1239.5	+9.5 %
Thin-Ply; 25.0 vol.-% SF	1556	1513.9	+2.8 %

Table 4: Comparison of the increase in bearing strength and damage initiation stress between the experimental and the simulation results

The improvement in the bearing strength compared to the respective Thick-Ply reference samples is 11.2 % within the simulation, which is below the experimentally measured increase of 18 %. One possible explanation for the lower improvement could be the in-situ strength, which is not yet implemented in the model within this study. Many studies have shown that the shear and transverse tensile strength is a function of the layer thickness. Both strengths increase with decreasing layer thickness [6]. The increase in shear and transverse tensile strength is expected to increase the bearing strength. Due to the hybridisation, the influence of the in-situ strength decreases. The difference between experiment and simulation in the hybrid specimens case is significantly lower.

In Figure 7, on the left-hand side, a stress-strain diagram represents the experimentally determined behaviour of a Thin-Ply reference (light blue) and a Thin-Ply specimen with 25 vol.-% stainless steel foil (dark blue). On the right side of Figure 7, two micrographs are shown above after the final failure. The left micrograph shows a Thin-Ply sample without stainless steel, and the right micrograph is a Thick-Ply sample with a steel content of 25 vol.-%. Both micrographs show more than one kink band. The formation of each kink band can be attributed to a stress drop in the stress-strain diagram. The progressive behaviour differs from the failure behaviour within the simulation. The first significant damage causes the final failure within the simulation. The two pictures below show the fibre rotation after the final failure. Red and blue areas represent broken fibres with a fibre rotation of 10° due to fibre kinking. On the left side is a Thin-Ply sample without stainless steel; on the right side is a Thick-Ply sample with a steel content of 25 vol.%. The steel layers are shown in grey. In the case of the Thick-Ply sample, the initiation of the kink band starts from the middle two 0° layers. The fibres of the 0° layers fail due to the large deformation by the kink band. As a result, the whole laminate fails. A similar phenomenon can be seen in the micrograph on the right. Five of the six 0° layers exhibit broken fibres.

However, the position of the kink band is not in the area of load application as in the simulation. The location of the kink band is behind the clamping area by the washers. To simulate the failure behaviour more accurately, the next step is to implement the tightening of the laminate. The simulation's failure pattern in the case of the Thin-ply specimen shows similar behaviour to the micrograph. A kink band is initiated across the whole specimen. But the kink band in the clamping area leads to final failure. In the experiment, a residual stiffness is given by the tightening of the washers, allowing compressive stresses to continue to be transferred, and the second kink band outside the area of the tightening leads to final failure, where the layers slide off after the formation of the kink band and the fracture of the fibres. However, a typical post-failure behaviour as it occurs after the first kink band cannot yet be simulated with the present model.
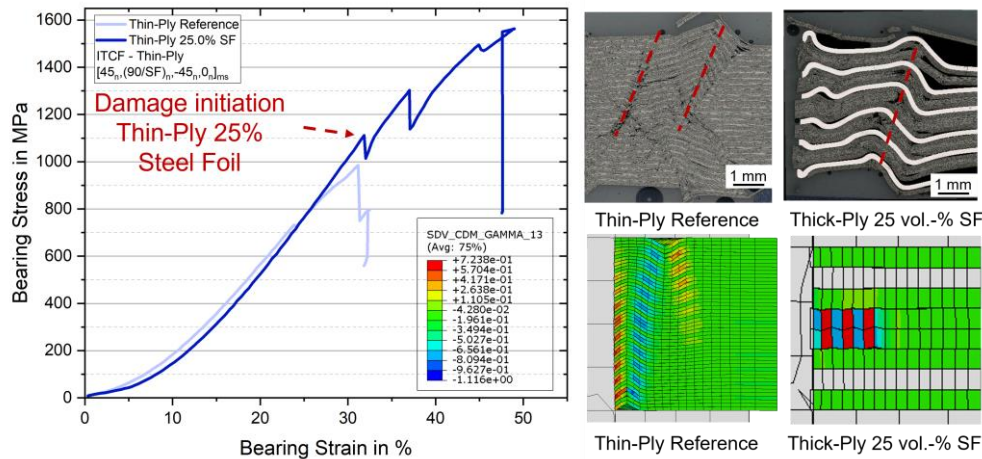

Figure 7: Left) Stress-Strain diagram of the progressive bearing behaviour of the hybrid Thin-Ply specimen, Right) Micrographs of the tested specimens

The simulations, as well as the experiments, show that fibre kinking leads to final failure. A significant influence on the initiation of fibre kinking is the compressive stress and the geometrical stability against buckling. The simulations showed that the initiation of kinking is in the 0° layers. Figure 8 presents the maximum compressive stress in fibre direction within the middle 0° layer as a function of the global bearing stress up to 1200 MPa. The graphs represent the Thin-Ply specimens with different steel contents. Comparing the reference specimen with the specimen with a local steel content of 25 vol.-%, the maximum compressive stress within the 0° layer is significantly higher at the same global bearing stress. Due to the isotropic material behaviour of the stainless-steel foils, higher stresses can be absorbed in the load direction in contrast to the substituted 90° layers. Therefore, the compressive stress of the middle 0° layer is lower. Lower compressive stresses within the 0° layer lead to a shift of the kinking initiation to higher global bearing stress. As expected, the compressive stress of the specimen with 12.5 vol.-% steel foil is between the reference sample and the sample with 25 vol.-% steel.

Furthermore, the curve of the samples with 6.25 vol.-% stainless steel is almost identical to the curve without stainless steel. This can be explained by the fact that only two 90° layers were substituted in the 2nd and 31st layers, respectively. Therefore, the influence of the outer steel layers on the compressive stress of the middle 0° layers is significantly lower.
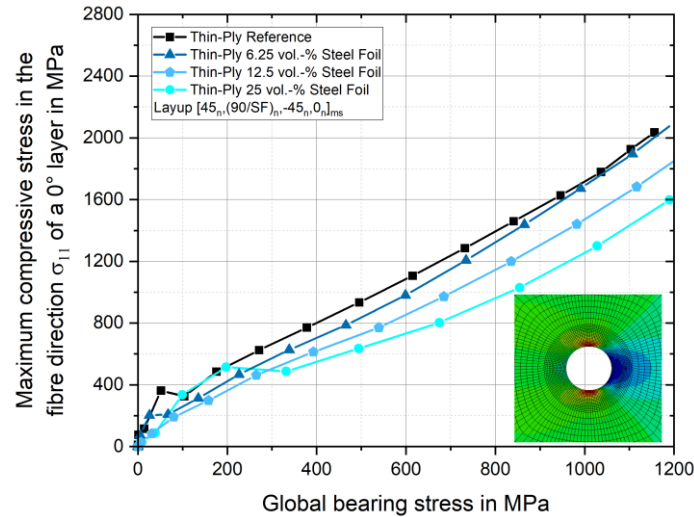
Figure 8: Maximum compressive stress in fibre direction σ_{11} of a $0°$ layer as a function of the global bearing stress

4   CONCLUSIONS

The aim of the present study was to investigate the influence of hybridisation by stainless steel patches in the area of load introduction of bolted joints depending on the layer thickness by numerical simulations. The damage model CompDam – DGD and the material parameters were validated against experimental results using a Thick-Ply specimen without stainless steel. The results showed that the stiffness of the joint and the bearing strength are very well represented. To investigate the influence of hybridisation, smaller FEM models were used to reduce the computation time. The results showed that the bearing strength increases with decreasing layer thickness. However, the increase in bearing strength was significantly lower than the increase in tensile and compressive strength. Improvements of up to 50 % were observed by substituting the $90°$ layers with stainless steel patches. The results indicate that if Thin-Ply laminates are used as a structural material in future applications, local hybridisation can significantly increase the lightweight performance. Regarding the failure behaviour, all configurations showed that fibre kinking leads to final failure. The initiation of the kink band always started from the $0°$ layers. However, as a result of the hybridisation, the kinking initiation shifted to higher bearing stresses. Due to the isotropic material properties of the stainless-steel foils, the foils absorb more compressive stresses in the load direction than the substituted $90°$ layers, which reduces the compressive stress within the $0°$ layers.

REFERENCES

[1] A. Wang, Z. Wang, Y. Zhao, Z. Chang, X. Shao, Y. Kang, Fatigue behaviour and failure mechanism of the thin/thick-ply hybrid laminated composite bolted joints, *Composite Structures*, 2022, pp. 115636 (doi: 10.1016/j.compstruct.2022.115636).

[2] A. Arteiro, C. Furtado, G. Catalanotti, P. Linde, P. P. Camanho, Thin-ply polymer composite materials: A review, *Composites Part A: Applied Science and Manufacturing*, **132**, 2020, pp. 105777 (doi: 10.1016/j.compositesa.2020.105777).

[3]   R. Amacher, J. Cugnoni, J. Botsis, L. Sorensen, W. Smith, C. Dransfeld, Thin ply composites: Experimental characterization and modeling of size-effects, *Composites Science and Technology*, **101**, 2014, pp. 121–132 (doi: 10.1016/j.compscitech.2014.06.027).

[4]   S. Sihn, R. Kim, K. Kawabe, S. Tsai, Experimental studies of thin-ply laminated composites, *Composites Science and Technology*, **67**, 2007, pp. 996–1008 (doi: 10.1016/j.compscitech.2006.06.008).

[5]   B. Kötter, J. Endres, J. Körbelin, F. Bittner, H.-J. Endres, B. Fiedler, Fatigue and fatigue after impact behaviour of Thin- and Thick-Ply composites observed by computed tomography, *Composites Part C: Open Access*, **5**, 2021, pp. 100139 (doi: 10.1016/j.jcomc.2021.100139).

[6]   P. P. Camanho, A. Fink, A. Obst, S. Pimenta, Hybrid titanium–CFRP laminates for high-performance bolted joints, *Composites Part A: Applied Science and Manufacturing*, **40**, 2009, pp. 1826–1837 (doi: 10.1016/j.compositesa.2009.02.010).

[7]   A. Arteiro, G. Catalanotti, J. Xavier, P. P. Camanho, Notched response of non-crimp fabric thin-ply laminates, *Composites Science and Technology*, **79**, 2013, pp. 97–114 (doi: 10.1016/j.compscitech.2013.02.001).

[8]   B. Kötter, K. Yamada, J. Körbelin, K. Kawabe, M. Nishikawa, M. Hojo, B. Fiedler, Steel foil reinforcement for high performance bearing strength in Thin-Ply composites, *Composites Part C: Open Access*, **4**, 2021, pp. 100085 (doi: 10.1016/j.jcomc.2020.100085).

[9]   A. Fink, P. P. Camanho, J. M. Andrés, E. Pfeiffer, A. Obst, Hybrid CFRP/titanium bolted joints: Performance assessment and application to a spacecraft payload adaptor, *Composites Science and Technology*, **70**, 2010, pp. 305–317 (doi: 10.1016/j.compscitech.2009.11.002).

[10] A. Crosky, D. Kelly, R. Li, X. Legrand, N. Huong, R. Ujjin, Improvement of bearing strength of laminated composites, *Composite Structures*, **76**, 2006, pp. 260–271 (doi: 10.1016/j.compstruct.2006.06.036).

[11] R. Li, N. Huong, A. Crosky, A. P. Mouritz, D. Kelly, P. Chang, Improving bearing performance of composite bolted joints using z-pins, *Composites Science and Technology*, **69**, 2009, pp. 883–889 (doi: 10.1016/j.compscitech.2008.12.005).

[12] Z. Hashin, Failure Criteria for Unidirectional Fiber Composites, *Journal of Applied Mechanics*, **47**, 1980, pp. 329–334 (doi: 10.1115/1.3153664).

[13] C. G. Davila, P. P. Camanho, C. A. Rose, Failure Criteria for FRP Laminates, *Journal of Composite Materials*, **39**, 2005, pp. 323–345 (doi: 10.1177/0021998305046452).

[14] J. Wang, T. Qin, N. R. Mekala, Y. Li, M. Heidari-Rarani, K.-U. Schröder, Three-dimensional progressive damage and failure analysis of double-lap composite bolted joints under quasi-static tensile loading, *Composite Structures*, **285**, 2022, pp. 115227 (doi: 10.1016/j.compstruct.2022.115227).

[15] A. Puck, H. Schürmann, Failure analysis of FRP laminates by means of physically based phenomenological models, *Composites Science and Technology*, **62**, 2002, pp. 1633–1662 (doi: 10.1016/S0266-3538(01)00208-1).

[16] X. Wang, Y. Wang, Y. Ji, H. Hu, D. Cao, K. Zheng, H. Liu, S. Li, Modeling Progressive Damage and Failure of Single-Lap Thin-Ply-Laminated Composite-Bolted Joint Using LaRC Failure Criterion, *Materials*, **15**, 2022, pp. 8123 (doi: 10.3390/ma15228123).

[17] F. Zhuang, A. Arteiro, R. P. Tavares, P. P. Camanho, P. Chen, Modelling damage in half-hole pin bearing cross-ply and angle-ply composite laminates, *Composite Structures*, **300**, 2022, pp. 116103 (doi: 10.1016/j.compstruct.2022.116103).

[18] F. A. Leone, A. C. Bergan, C. G. Dávila, CompDam - Deformation Gradient Decomposition (DGD), v2.5.0, https://github.com/nasa/CompDam/_DGD, 2019([Online]. Available at: https://github.com/nasa/CompDam/_DGD).

[19] F. A. Leone, Deformation gradient tensor decomposition for representing matrix cracks in fiber-reinforced materials, *Composites Part A: Applied Science and Manufacturing*, **76**, 2015, pp. 334–341 (doi: 10.1016/j.compositesa.2015.06.014).

[20] B. Budiansky, Micromechanics, *Computers & Structures*, **16**, 1983, pp. 3–12 (doi: 10.1016/0045-7949(83)90141-4).

[21] B. Budiansky, N. A. Fleck, Compressive failure of fibre composites, *Journal of the Mechanics and Physics of Solids*, **41**, 1993, pp. 183–211 (doi: 10.1016/0022-5096(93)90068-Q).

[22] A. Bergan, A Three-Dimensional Mesoscale Model for In-Plane and Out-of-Plane Fiber Kinking, In: AIAA Scitech 2019 Forum. San Diego, California: American Institute of Aeronautics and Astronautics; 2019

[23] C. G. Dávila, From S-N to the Paris Law with a New Mixed-Mode Cohesive Fatigue Model, 2018

[24] A. Bergan, M. Herráez, C. González, C. Lopes, Development of a Mesoscale Finite Element Constitutive Model for Fiber Kinking, In: 2018 AIAA/ASCE/AHS/ASC Structures, Structural Dynamics, and Materials Conference. Kissimmee, Florida: American Institute of Aeronautics and Astronautics; 2018

[25] F. A. Leone, Representing Matrix Cracks through Decomposition of the Deformation Gradient Tensor in Continuum Damage Mechanics Methods, Copenhagen: 2015. p. 12.

[26] C. A. Rose, C. G. Davila, F. A. Leone, Analysis Methods for Progressive Damage of Composite Structures, 2013

[27] B. Budiansky, N. A. Fleck, J. C. Amazigo, On kink-band propagation in fiber composites, *Journal of the Mechanics and Physics of Solids*, **46**, 1998, pp. 1637–1653 (doi: 10.1016/S0022-5096(97)00042-2).

[28] W. Ramberg, W. R. Osgood, Description of Stress-Strain Curves by Three Parameter, 1943

[29] D30 Committee, Test Method for Bearing Response of Polymer Matrix Composite Laminates, ASTM International

[30] Yamada K., Nishikawa M., Kotter B., Matsuda N., Kawabe K., Fiedler B., Hojo M., Effect of Ply-level Hybridization and Insertion of Metal Layers on Impact Damage Modes and Compression Strength after Impact of Thin-ply Composite Laminates, *Journal of the Japan Society for Composite Materials*, **46**, 2020, pp. 104–114 (doi: 10.6089/jscm.46.104).

[31] K. Yamada, B. Kötter, M. Nishikawa, S. Fukudome, N. Matsuda, K. Kawabe, B. Fiedler, M. Hojo, Mechanical properties and failure mode of thin-ply fiber metal laminates under out-of-plane loading, *Composites Part A: Applied Science and Manufacturing*, **143**, 2021, pp. 106267 (doi: 10.1016/j.compositesa.2020.106267).

[32] D30 Committee, Test Method for Mode I Interlaminar Fracture Toughness of Unidirectional Fiber-Reinforced Polymer Matrix Composites, ASTM International

[33] D30 Committee, Test Method for Determination of the Mode II Interlaminar Fracture Toughness of Unidirectional Fiber-Reinforced Polymer Matrix Composites, ASTM International

[34] E28 Committee, Test Methods of Tension Testing of Metallic Foil, ASTM International

[35] G. Johnson, W. Cook, A constitutive model and data for metals subjected to large strains, strain rates, and high pressures, 1983.